ELSEVIER

International Journal of Refrigeration 23 (2000) 127–140

REVUE INTERNATIONALE DU FROID
INTERNATIONAL JOURNAL OF
refrigeration

www.elsevier.com/locate/ijrefrig

Analysis of the air flow in a cold store by means of computational fluid dynamics

M.L. Hoang*, P. Verboven, J. De Baerdemaeker, B.M. Nicolaï

Department of Agro-Engineering and -Economics, K.U. Leuven, Kardinaal Mercierlaan 92E, B-3001 Heverlee, Belgium

Received 14 January 1999; received in revised form 19 July 1999; accepted 22 July 1999

Abstract

Airflow inside a cold store is investigated using computational fluid dynamics. The airflow model is based on the steady state incompressible, Reynolds-averaged Navier–Stokes equations. The turbulence is taken into account using a $k-\varepsilon$ model. The standard as well as the Renormalisation-Group (RNG) version of the $k-\varepsilon$ model is investigated. The forced-circulation air cooler unit is modelled with an appropriate body force and resistance, corresponding to the characteristics of the fan and the tube-bank evaporator. The finite volume method of discretisation is used. The validation of the model has been performed by a comparison of the calculated time-averaged velocity magnitudes with the mean velocities measured by means of a hot-film type omni-directional velocity sensor. A relative error on the calculated air velocities of 26% was observed. The RNG $k-\varepsilon$ model does not help to improve the prediction of the recirculation. Both a finer grid and enhanced turbulence models are needed to improve the predictions. © 2000 Elsevier Science Ltd and IIR. All rights reserved.

Keywords: Cold store; Air distribution; Simulation; Computerized

Analyse du débit d'air dans un entrepôt frigorifique à l'aide de la dynamique des fluides informatisée

Résumé

Le débit d'air à l'intérieur d'un entrepôt frigorifique a été étudié à l'aide de la dynamique des fluides informatisée (CFD). Le modèle du débit d'air est fondé sur le régime permanent incompressible et des équations de Navier-Stokes avec les moyens calculés à l'aide de la méthode Reynolds. On tient compte de la turbulence à l'aide d'un modèle k−ε. La norme, et la version du Groupement-Rénormalisation (RNG) du modèle k−ε, sont étudiées. On modélise le refroidisseur d'air forcé en utilisant une force volumique et résistance appropriées, correspondant aux caractéristiques du ventilateur et de l'évaporateur multitubulaire. On a employé la méthode de discrétisation du volume fini. Ce modèle a été validé par la comparaison des magnitudes des vitesses moyennes en fonction du temps, avec des mesures effectuées à l'aide d'un capteur de type film chaud multidirectionnel. Pour les calculs de la vitesse de l'air, l'erreur relative a été de 26 %. Le modèle RNG k−ε n'améliore pas la prévision de la recirculation. Afin d'améliorer les prévisions, il sera nécessaire d'utiliser une grille plus fine et des modèles de turbulence affinés. © 2000 Elsevier Science Ltd and IIR. All rights reserved.

Mots clés: Entrepôt frigorifique; Distribution d'air; Simulation; Informatique

* Corresponding author. Tel.: +32-16-321922; fax: +32-16-321994.
E-mail address: hoang.lan@agr.kuleuven.ac.be (M.L. Hoang)

PII: S0140-7007(99)00043-2

Nomenclature

a	geometrical factor
b	geometrical factor
C	constant in heat exchanger resistance equation
C_1, C_2, C_3	experimental coefficient in the fan model
$C_{1\varepsilon}$	constant in production term of ε-equation
$C_{2\varepsilon}$	constant in dissipation term of ε-equation
C_μ	constant in turbulent viscosity formula
D_1, D_2	distances between two adjacent tubes in the two directions in the cooler (m)
d	diameter of the tube in the cooler (m)
E	average difference between the measured and the calculated velocities
k	turbulence kinetic energy (m^2/s^2)
ΔL	length of the cooler unit in z direction (m)
m	geometry parameter
P	turbulence energy production (kg/ms^3)
Ps	shear part of turbulence energy production (kg/ms^3)
p	pressure (Pa)
S	source term in the momentum equation (N/m^3)
T	temperature (°C)
t	time (s)
U	velocity vector (m/s)
U_l	superficial velocity in the cooler (m/s)
U^i_{CFD}	average calculated velocity at position i (m/s)
U^i_{exp}	average measured velocity at position i (m/s)
v	velocity component (m/s)
y^+	dimensionless normal distance to wall
z	number of tube rows

Greek letters

β	constant in ε-equation in RNG $k-\varepsilon$ model
ε	turbulence energy dissipation (m^2/s^3)
η	term in ε equation in RNG $k-\varepsilon$ model
η_0	constant in ε equation in RNG $k-\varepsilon$ model
μ	viscosity (kg/ms)
ρ	density (kg/m^3)
σ_k	turbulent Prandtl number for k
σ_T	turbulent Prandtl number for ε

Subscripts

eff	effective value of parameter
i	index of Cartesian components
RNG	index for RNG $k-\varepsilon$ model
T	turbulent part of parameter

1. Introduction

A uniform cooling and cold storage of fresh produce are difficult to obtain in industrial cooling rooms because of an uneven distribution of the airflow [1,2]. The airflow distribution is dependent on the produce, the cooling medium, the geometry and characteristic of the cooling room. The velocity distribution can be determined based on the conservation equations for mass and momentum. An analytical solution can be found only in simple cases. The variables can be examined experimentally [3], but this is a tedious, costly, time-consuming method and furthermore, it is only applicable to existing storage rooms. It can, hence, not be used to optimise the storage room in an early phase of the design. With the increasing availability and power of computers together with efficient solution algorithms and processing facilities, the governing fluid flow equations can now be solved numerically. The technique of Computational Fluid Dynamics (CFD), which uses computers for solving fluid flow problems, is very powerful and spans a wide range of industrial and non-industrial application areas. Several user-friendly software packages are available such as PHOENICS (Flowsolve, London), CFX (AEA, Harwell, UK), STAR-CD (CD, London), FLUENT/FIDAP (Lebanon, USA).

Wang and Touber [2] used PHOENICS to model the airflow pattern, temperature and moisture distribution. In a refrigerated room, the diffusion term was neglected and the equations for heat and mass transport were linearized. The air velocities and humidity were not measured, which put a considerable limit on the reliability of this model. Van Gerwen and Van Oort [4,5] also applied PHOENICS to simulate the velocity and temperature distribution in a refrigerated room. The validation was done for the airflow velocity, airflow patterns, static pressure and temperature of the air and the product. However, no data were given. Furthermore no information was reported about how the boundary conditions were applied. Mirade et al. [6] applied CFD to simulate the airflow in a meat chiller. The validation efforts were considerable but modelling of the fan action through an appropriate boundary condition remained a problem. Marriotti et al. [7] used the finite element method to simulate the air distribution in a refrigerated

room with different air inlet conditions. There was no validation for the model.

In this study, CFD is used to develop and solve a mathematical model, which describes the steady, isothermal 3D forced airflow in a cold store. The purpose of the cold store is the long-term storage of fruits and vegetables in individual storage units, called pallet-boxes or palloxes. The specific features of such a cold store are:

- large blockages of the airflow by means of the stack of palloxes.
- inclusion of the air-conditioning unit inside the room, which complicates the definition of boundary conditions. Rather than a simple inlet–outlet configuration, the air-conditioning unit must be treated as a momentum source term.
- low air velocities from nearly zero to ± 3 m/s combined with turbulence in the transition region and in a complicated geometry.

It should also be noticed that the sector of fresh fruits and vegetables has very narrow profit margins. The purpose of this study is therefore to:

- Build a CFD model that is affordable in terms of computation time, using available CFD techniques in a commercial code (CFX, Harwell, UK).
- Have an extensive comparison of the CFD results with measurements performed with a sensor that has a good cost/accuracy balance and can be applied in industrial operating condition.

Based on this study, it will be decided whether current methods allow the food engineer to use CFD to optimise cold store designs. It is left to the fundamental researchers in CFD and measurement techniques to develop enhanced techniques.

2. Methods

2.1. Governing equations

The governing equations based on the conservation of mass and momentum of a Newtonian fluid flow and applied to an infinitesimal small volume in a Cartesian co-ordinate system (x, y, z) are, using the Reynolds averaged formulation:

$$\frac{\partial \rho}{\partial t} + \mathrm{div} U = 0 \tag{1}$$

$$\frac{\partial(\rho \upsilon_i)}{\partial t} + \mathrm{div}(\rho U \upsilon_i) = \mathrm{div}(\mu_{\mathrm{eff}} \,\mathrm{grad}\,\upsilon_i) - \frac{\partial P'}{\partial x_i} + S_i \tag{2}$$

$$\rho = \rho(p, T) \tag{3}$$

$$\mu_{\mathrm{eff}} = \mu + \mu_T \tag{4}$$

In these formulae, $U(\upsilon_1, \upsilon_2, \upsilon_3)$ is the velocity vector, consisting of the three components $\upsilon_1, \upsilon_2, \upsilon_3$ (m/s); p is the pressure (Pa), T is temperature (°C). The density ρ(kg/m^3) and the laminar viscosity μ(kg/ms) are the only fluid properties involved; μ_T and μ_{eff} are the turbulent and effective viscosity, respectively. The sources S_i contain further contributions of the viscous stress terms and can contain additional body forces. The airflow at a constant temperature in the room is considered. Constant air properties are considered: $\rho = 1.1941$ kg/m^3 and $\mu = 181.1 \times 10^{-7}$ Ns/m^2.

2.2. Turbulence models

The $k-\varepsilon$ models are the most widely validated turbulence models in literature and are the standard models to use in the commercial codes. However, they have limitations, which necessitates the validation of the CFD results. The $k-\varepsilon$ model uses an eddy-viscosity hypothesis for the turbulence, expressing the turbulent stresses as an additional viscous stress term [Eq. (4)]. In the $k-\varepsilon$ model, the turbulent viscosity is expressed in terms of two variables: the turbulence kinetic energy k and its dissipation rate ε. In this model, the k and ε equations are of a similar conservation format, containing convective and diffusive terms.

2.2.1. The standard k−ε model

In the standard $k-\varepsilon$ model, the production and destruction terms in the ε equation contain empirical constants. The resulting equations are similar to the governing flow equations [17]:

$$\mu_T = C_\mu \rho \frac{k^2}{\varepsilon} \tag{5}$$

$$p' = p\frac{2}{3}\rho k \tag{6}$$

$$\frac{\partial \rho k}{\partial t} + \mathrm{div}(\rho U k) - \mathrm{div}\left[\left(\mu + \frac{\mu_T}{\sigma_k}\right)\mathrm{grad}(k)\right] = P - \rho\varepsilon \tag{7}$$

$$\frac{\partial \rho \varepsilon}{\partial t} + \mathrm{div}(\rho U \varepsilon) - \mathrm{div}\left[\left(\mu + \frac{\mu_T}{\sigma_\varepsilon}\right)\mathrm{grad}(\varepsilon)\right] = C_{1\varepsilon}\frac{\varepsilon}{k}P - C_{2\varepsilon}\rho\frac{\varepsilon^2}{k} \tag{8}$$

where P is a term containing the turbulence production due to the stresses in the flow. The standard $k-\varepsilon$ model is the most widely validated turbulence model available, but it contains five empirical constants (C_μ, C_1, C_2, σ_k, σ_ε). However, except for complex flow close to walls, the standard values for these constants are regarded as

suitable for a wide range of conditions [8] and during this study these constants were not changed:

$$C_\mu = 0.09; \sigma_k = 1.0; \sigma_\varepsilon = 1.3; C_{1\varepsilon} = 1.44; C_{2\varepsilon} = 1.92 \quad (9)$$

Near walls the equations do not hold, and standard logarithmic wall profiles are implemented. In this way the need to integrate the model equations up to the wall is avoided and coarser numerical grids can be used. The details of this approach are not outlined here, but can be found in the textbook by Versteeg and Malalasekera [8]. An important variable is y^+, a dimensionless distance normal to the wall. The value of y^+ determines in which region of the boundary layer the first grid node is situated. The log-law is valid only for $y^+ > 30$. One should bare in mind that the log-law is developed for parallel flow over a smooth flat plate with no adverse pressure gradients.

2.2.2. RNG $k-\varepsilon$ model

The RNG $k-\varepsilon$ model [9] is obtained via a statistical mechanics approach, in which the small scale motions are systematically removed from the governing equations by expressing their effects in terms of larger scale motions and a modified viscosity. The advantage of this approach is that the constants in the equations are calculated explicitly. Additionally, a new term appears in the ε-equation, which account for anisotropy in strongly strained turbulent flows. This term is incorporated through a modelled constant in the production term, based on the equilibrium assumption that production equals dissipation, restricting the RNG $k-\varepsilon$ model to a coarse grid approach near walls. The same default wall functions as in the standard $k-\varepsilon$ model are valid in this case. The ε equation is:

$$\frac{\partial \rho\varepsilon}{\partial t} + \mathrm{div}(\rho U\varepsilon) - \mathrm{div}\left[\left(\mu + \frac{\mu_T}{\sigma_\varepsilon}\right)\mathrm{grad}(\varepsilon)\right] = (C_{1\varepsilon} - C_{1\mathrm{RNG}})\frac{\varepsilon}{k}P - C_{2\varepsilon}\rho\frac{\varepsilon^3}{k} \quad (10)$$

$$C_{1\mathrm{RNG}} = \frac{\left(1 - \frac{\eta}{\eta_0}\right)}{(1 + \beta\eta^3)} \quad (11)$$

$$\eta = \left(\frac{P_s}{\mu_T}\right)^{0.5}\frac{k}{\varepsilon} \quad (12)$$

where η_0 and β are additional model constants, which are equal to 4.38 and 0.015, respectively, and P_S is the shear part of the production. The standard values of the other constants are regarded as suitable for this application:

$$C_\mu = 0.085; \sigma_k = 0.7179; \sigma_\varepsilon = 0.7179; C_{1\varepsilon} = 1.42; C_{2\varepsilon} = 1.68 \quad (13)$$

The k equation is the same format as in the standard $k-\varepsilon$ model, and the same wall profiles are applied.

2.3. Model of the fan and the cooler unit

The fan and the cooler unit are modelled as a dynamic source term in Eq. (2) interacting with the flow in the cold store. Experimental input is only required initially in the model formulation for the determination of the head-capacity curve of the fan and the pressure drop of the heat exchanger.

The fan model (Fig. 1) is formulated based on the fan characteristic, provided by the cooler supplier:

$$\Delta p = C_1 + C_2|U_l| + C_3 U_l^2 \quad (14)$$

where Δp is the total pressure (N/m^2); U_1 is the superficial velocity (m/s), equal to the volume flow rate divide by the cross section of the cooler unit and

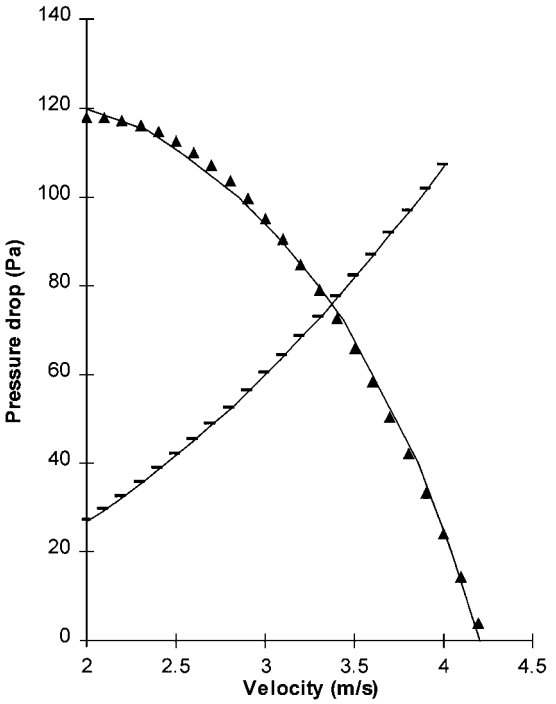

Fig. 1. Models of the cooler resistance (hyphen) and the fan with a rotation speed of 1380 rev/min: model (triangles) and the supplier data (continuous curve).

Fig. 1. Modèles de la résistance du refroidisseur (courbe avec traits) et du ventilateur ; pour une vitesse de rotation de 1380 tours / minute : le modèle (courbe avec triangles) et les données du fabricant (courbe continue).

C_1, C_2, C_3 are experimental coefficients, obtained from the characteristic curve and equal to 18.65, 98.04 and −24.18, respectively, for the velocity range from 2 to 4.2 m/s (Fig. 1).

The heat exchanger resistance, introduced by Zukauskas and Ulinskas [10], is modelled as (Fig. 1):

$$\Delta p = -Cmz\rho\frac{a^2}{2(a-1)^2}|U_1|U_1 \tag{15}$$

where Δp is the pressure drop due to the resistance of the cooler tubes (N/m^2); C is a constant factor and equal to 0.35; z is the number of tube rows ($z=10$); m is a geometry parameter:

$$m = 1.004\left(\frac{a-1}{b-1}\right)^{-0.539} \tag{16}$$

with

$$a = \frac{D_1}{d}; b = \frac{D_2}{d} \tag{17}$$

Here, d is the diameter of the tube and equal to 0.016 m; D_1 and D_2 are the distances between two adjacent tubes in the two directions. In this case, D_1 is equal to D_2 and equal to 0.049 m, so the parameter m is equal to 1.004.

The models of the fan and the cooler are summed and applied to the momentum equation as a local source in the direction of the local flow in the cooler unit:

$$S = \frac{\Delta p}{\Delta L} \tag{18}$$

with ΔL is the length of the cooler unit, $\Delta L = 0.785$.

2.4. Model of the cold store

An unloaded cold store as well as a loaded one is modelled. The loaded room contains four palloxes (empty wooden pallet boxes sealed off at the top) with the dimension 1.14 m wide, 1.14 m long and 0.75 m high. The cold store that is modelled has the dimensions 2.5 m high, 2.7 m wide and 4.5 m deep and includes two coolers on the ceiling (Fig. 2a) at the back of the room. The 3D geometry is built up from prismatic blocks, which cover the different zones of the cold store. The room loaded with four palloxes consists of 459 blocks.

The geometry of the fan and the tube heat exchanger in the cooler are not modelled. The cooler is modelled as a block covering the cooler dimensions, in which the source term (18) is applied. The walls of the cooler are defined at the block faces. The humidifier, which is located in front of the cooler is modelled as a solid block: the velocity equations are not solved here and the solid block faces are walls where the velocity becomes zero. Inside the palloxes, the velocity equations are not solved and the pallox surfaces are defined as walls where the velocity becomes zero.

2.5. Numerical solution of the model equations

The popular finite volume method of discretisation is used in this study. All the equations are integrated over each small control volume around discrete points in the flow domain. A body-fitted structured grid covers the geometry. Two different grid resolutions have been studied: 42 236 control volumes and 167 152 control volumes. A non-uniform grid is used to reduce the number of control volumes leading to a shorter calculation time. The grid is refined close to the walls, in between the palloxes and inside the cooler. The refinement is gradual to avoid large errors, which can occur in

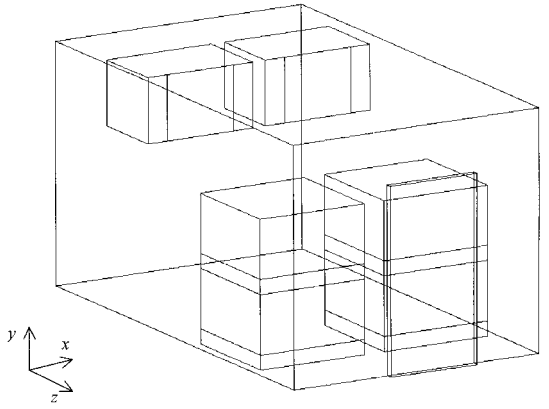

(a)

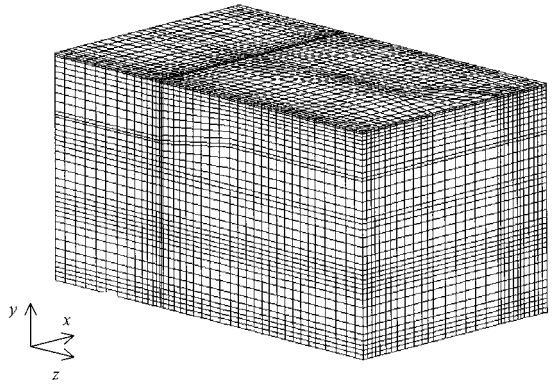

(b)

Fig. 2. (a) Geometry of the cold store with four palloxes and (b) the block-structured body fitted finite volumes grid.

Fig. 2. Géométrie de l'entrepôt frigorifique avec quatre pallox (a) et structuration avec grille pour volumes finis (b).

the calculation when adjacent control volumes differ too much in size. For the coarse grid, the y^+ is ranging from 50 to 400, for the fine grid the y^+ is in the range of 30 to 100. After integration, the resulting terms are discretised with finite difference approximations. The resulting system of non-linear equations is solved by means of an iterative solution algorithm provided by the computer code CFX [11]. Hybrid differencing is applied since it exploits the favourable properties of the upwind and central differencing schemes. It switches to the second

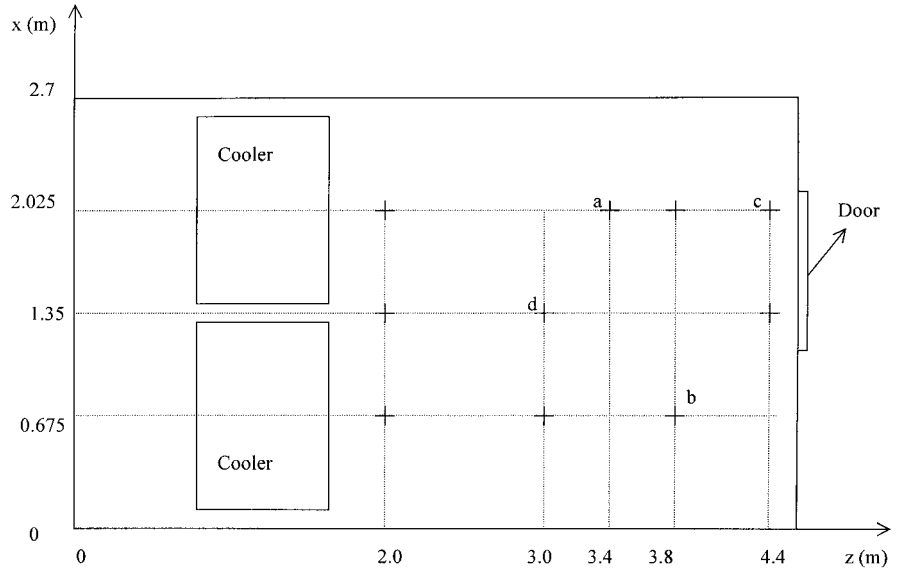

Fig. 3. Horizontal cross section of the empty room with the location of the vertical lines (+) where the velocities have been measured. The letters a to d indicate the positions corresponding to the graphs given in Fig. 7.

Fig. 3. Schéma de la chambre froide vide avec l'emplacement des axes verticaux (+) où les vitesses ont été mesurées. Les lettres a à d indiquent les positions correspondant aux courbes données par la Fig. 7.

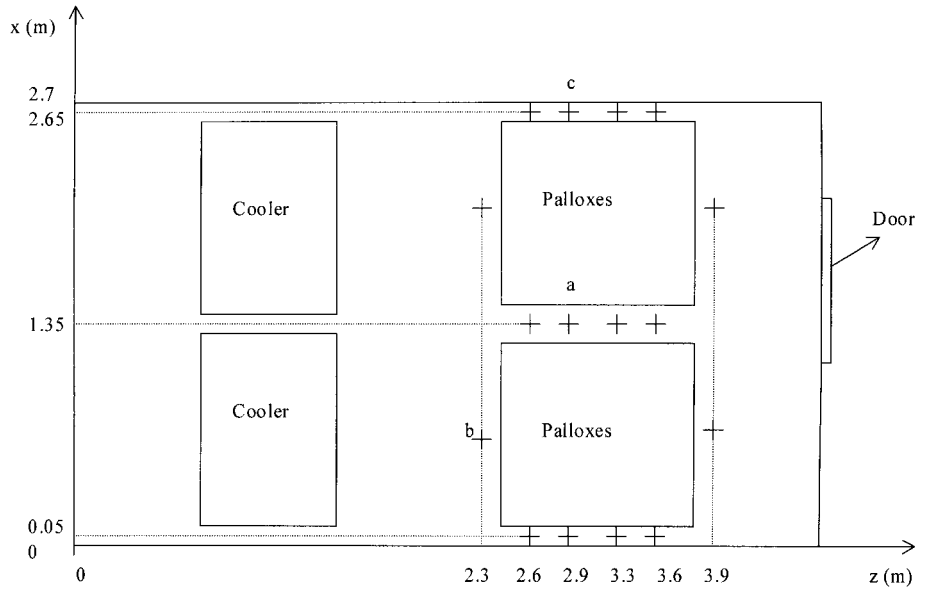

Fig. 4. Horizontal cross section of the loaded room with the location of the vertical lines (+) where the velocities have been measured. The letters a, b, c, indicate the positions corresponding to the graphs given in Fig. 9.

Fig. 4. Schéma de la chambre froide avec contenu, donnant l'emplacement des axes verticaux (+) où les vitesses ont été mesurées. Les lettres a, b et c indiquent les positions correspondant aux courbes données par la Fig. 9.

order upwind differencing when central differencing produces inaccurate results on coarse grids and at high velocities. The scheme is fully conservative and bounded and is known to produce physically realistic solutions [8].

For turbulent non-linear problems a steady state simulation rarely converges and a transient-like procedure must be applied. Implicit time stepping with sufficiently small step sizes (smallest size of the control volume divided by the velocity) led to a converged steady state solution. A total of 1300 steps, each solved for 15 iterations, were needed. The total calculation time ranged from 70 to 100 h on a HP 9000 C 160 workstation with 128 Mb RAM for the coarse grid. The absolute mass equation residuals in the main part of the flow domain reduced to the range of 10^{-7}–10^{-9} kg/s in each control volume, or 10^{-5} kg/s in total, which is 6 10^{-4} % of the fan flow rate. This indicates that the equations converged to a steady state solution. High residuals were encountered near the inlet of the cooler unit. The local grid refinement study revealed that this local error in the solution did not effect the main airflow pattern in the room.

2.6. Velocity measurement technique

There are several techniques available for quantitative, local velocity measurement such as laser-Doppler anemometry, sonic anemometry, vane anemometry, pitot tubes and thermal anemometry. A high accuracy can be obtained with laser-Doppler anenometry but it is very expensive and the laser beams must be able to penetrate the room from outside. In order to have a sensor, which can be used in industrial operating conditions with the best balance between cost and accuracy, an omni-directional hot film velocimeter (TSI 8475, St. Paul, MN) was used. The spherical probe tip is ideal for unknown or varying flow direction. The velocity range of the sensor is 0.05 to 2.5 m/s. The calibrated accuracy is 3.0% of the reading or 1.0% of full scale of the selected range of 2.5 m/s, which was assured by a certificate from the supplier. The accuracy at the low end of the range is therefore limited, due to the effects of buoyancy along the hot sphere and, if the flow is turbulent, the positive averaging of fluctuations (the sensor has no directional respons). The transducer is connected to a portable PC with a DAS-1400 data acquisition card (Keithley, Cleveland, OH). The software TESTPOINT 3.0 (Billerica, MA) was used to interface with the data acquisition. At each point the time-averaged velocity was determined from measurement with a frequency of 5 Hz (time constant of the sensor is 5 s) and averaged over a 5-minute period. The time constant is not sufficient to capture high frequency fluctuations, so no information was gathered on turbulence. In fact, velocity measurements at low velocities remain a tedious task, and, according to Chen et al. [12], no ideal instrument has yet been developed for the measurement of low velocities. Accuracy problems of omni-directional sensors is discussed by Melikov [13]. The measurements have been carried out at multiple points on different vertical lines in the empty room (Fig. 3) as well as in the loaded room (Fig. 4). A total of more than 600 points have been scanned (200 in the empty room and 400 in

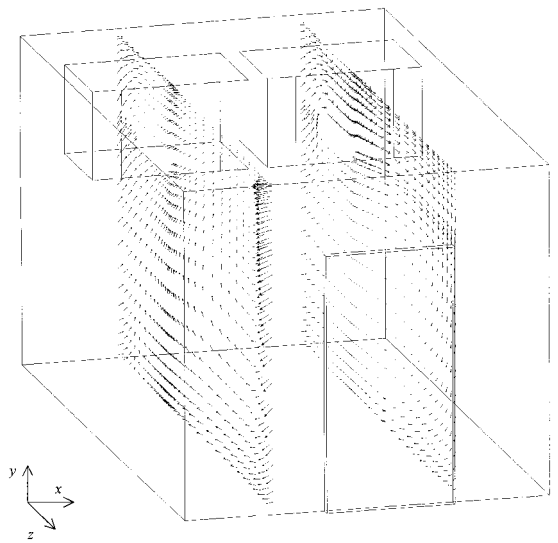

Fig. 5. Visualisation of the calculated air flow in the empty room.

Fig. 5. Visualisation du débit d'air calculé : chambre froide vide.

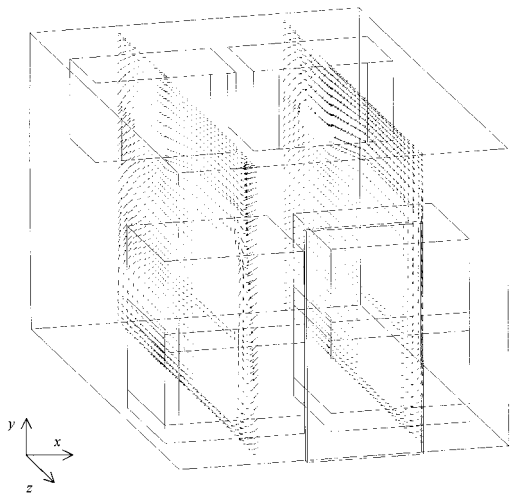

Fig. 6. Visualisation of the calculated air flow in the loaded room.

Fig. 6. Visualisation du débit d'air calculé : chambre froide avec contenu.

the loaded room). The overall accuracy of the CFD calculations is calculated as the average of the absolute differences between the time-averaged velocity magnitude from the CFD calculation and the measurement at each position, divided by the average velocity magnitude in the room obtained from the measurements, and is expressed as:

$$E = \frac{\sum_{i=1}^{n} |U^i_{\mathrm{CFD}} - U^i_{\mathrm{exp}}|}{\sum_{i=1}^{n} U^i_{\mathrm{exp}}} \times 100 \tag{19}$$

where U^i_{CFD} is the average velocity at position i from the CFD calculation, U^i_{exp} is the average velocity at position

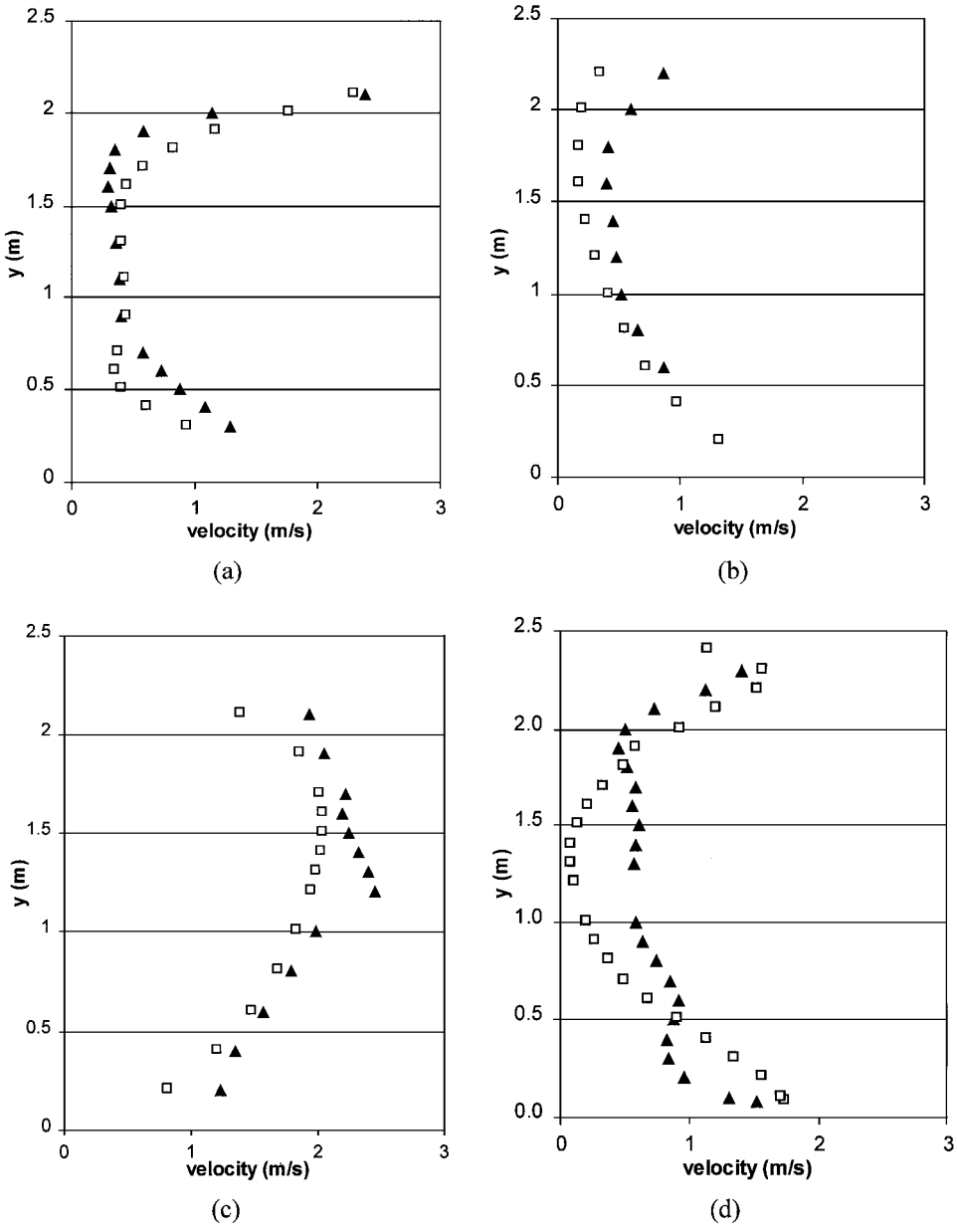

Fig. 7. Comparison between measured (black triangles) and calculated (clear squares) velocity magnitudes in different vertical lines in the empty room: a, b c, d are the positions shown in Fig. 3.

Fig. 7. Comparaison entre les magnitudes des vitesse mesurées (triangles noirs) et calculées (carrés blancs) de divers axes verticaux dans la chambre vide : a, b, c et d sont les positions montrées en Fig. 3.

i from the measurement and n is number of measurement positions.

3. Results and discussions

For the empty room, the model solution reached an equilibrium for an air flow of 4800 m^3/h, which is 5% lower than the value derived from the design pressure drop of the heat exchanger unit (78 Pa) and the head-capacity curve of the propeller fan, rotating at 1380 rev/min. When the room is loaded with four palloxes, the calculated air flow rate was 5.5% lower than the derived value. This indicates that the resistance caused by the palloxes is very small compared to the resistance of the cooler, for this configuration.

3.1. Grid refinement

The grid refinement has been carried out with two grid resolutions: 42 000 and 16 7000 control volumes for a loaded room. The results show a small improvement of prediction (23% error for the fine grid compared to 26% error for the coarse). The refinement was not sufficient to obtain a doubling of the number of subdivisions in each direction, due to the limitation of the computation power and the calculation time (7 days for the grid resolution of 167 000 control volumes). The results discussed in this text are based on the simulations, which have been done for the coarse grid only. However, the grid refinement study already reveals the limited possibilities of accurate CFD simulations of large-scale applications on an affordable computer system. With the development of faster and cheaper computers, this should no longer be a hurdle in the future.

3.2. Empty room

Only one of the two coolers operates in normal conditions. Therefore, the flow pattern is non-symmetrical in the room. The resulting pattern according to the model

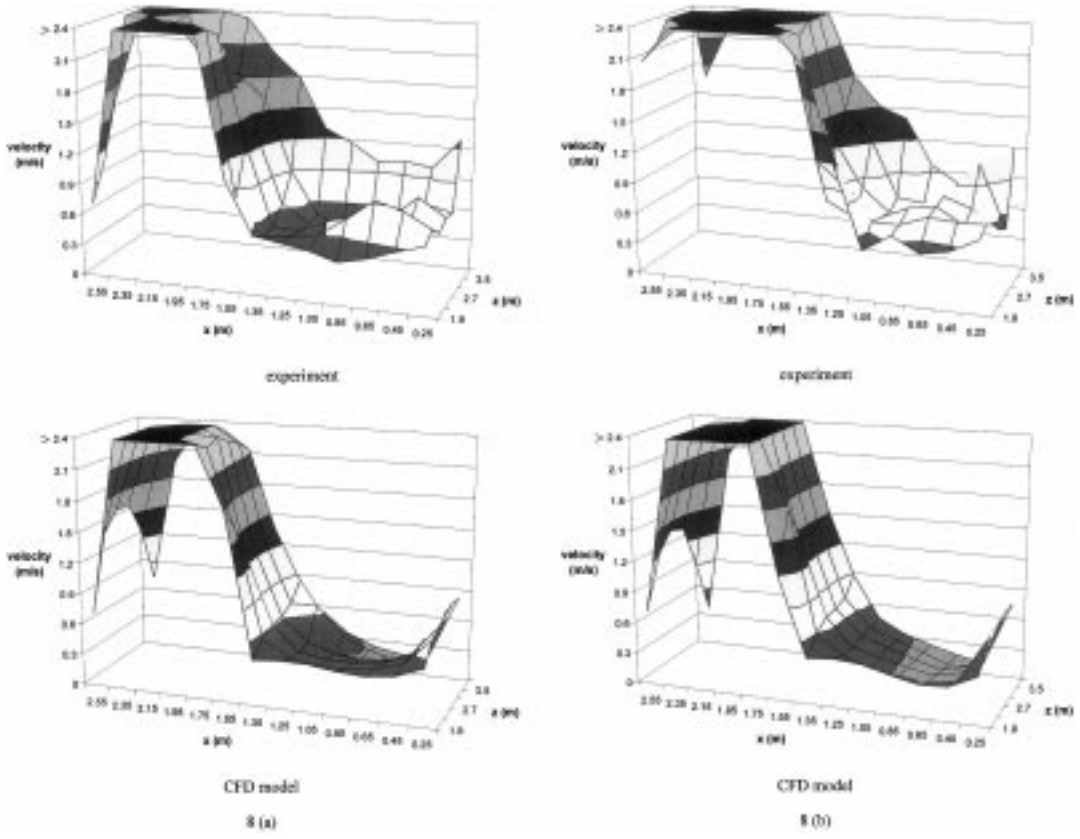

Fig. 8. Comparison between measured and calculated velocity magnitudes in an empty room at a height of 2.05 m (a) and 2.23 m (b), the x and z dimensions correspond to the dimensions in Fig. 3.

Fig. 8. Comparaison des vitesses calculées et mesurées dans une chambre vide à une hauteur de 2,05 m (a) et 2,23 m (b), les dimensions x et z correspondent aux dimensions mentionnées dans la Fig. 3.

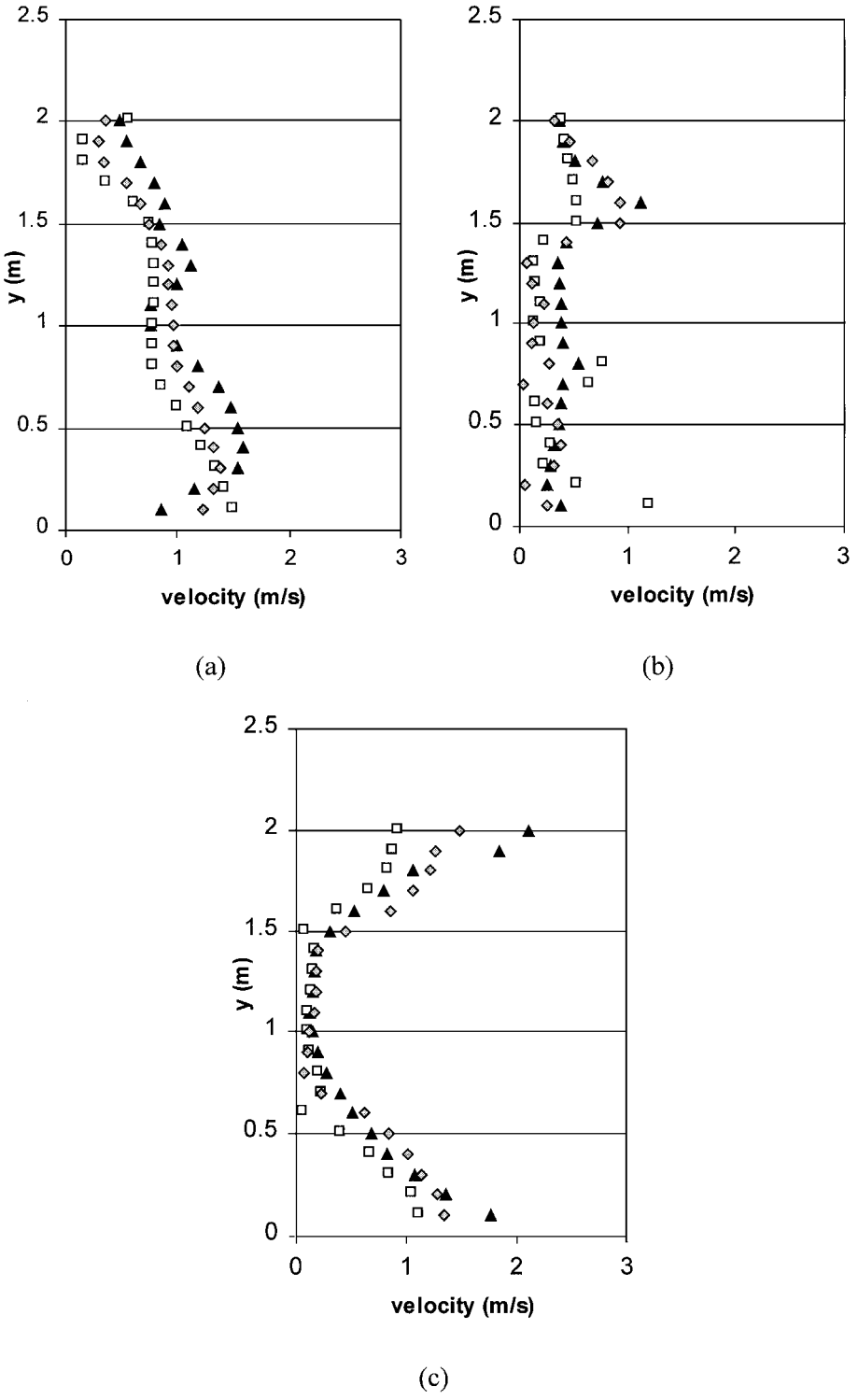

Fig. 9. Comparison between measured (black triangles) and calculated velocity magnitudes with the default model (clear squares) and spread-out model (grey diamonds) in different vertical lines in the room; a, b, c are the positions shown in Fig. 4.

Fig. 9. Comparaison entre les vitesses mesurées (triangles noirs) et calculées à l'aide du modèle par défaut (carrés blancs) et le modèle étalé (losanges gris) dans les axes verticaux de la chambre ; a, b et c sont des positions que montre la Fig. 4.

is as follows (Fig. 5). The air coming out of the cooler is accelerated, reaches the ceiling and spreads out. The air moves to the front where it flows downwards and returns to the back of the room with a high velocity close to the floor. Also at the opposite side of the room, the air is forced backwards with a high velocity near the side wall.

The validation of the calculated flow pattern is assessed by comparing the calculated and the measured velocities. In Fig. 7, some representations chosen for their relevance concerning the assessment of the airflow calculations are given. It can be seen that high velocities are encountered near the ceiling in front of the cooler unit (Fig. 7a). The large velocities near the floor are detected as well. In front of the non-operating cooler unit, the air moves at lower velocities near the ceiling and a more even vertical velocity distribution is established (Fig. 7b). Near the front side of the room, higher velocities are found than towards the cooler. Velocities are higher than 1 m/s (Fig. 7c), compared to the low velocities of 0.5 m/s in front of the cooler at mid height (Fig. 7a). These large velocities result from the large airflow near the ceiling, which is coming down along the front wall. In the centre of the room (Fig. 7d), again large velocities are found near the floor and ceiling and generally lower velocities at mid height.

Besides of this qualitative agreement, large local differences can be distinguished between the actual velocities and the calculations. The real velocity may at some places be twice as large as the calculated one (Fig. 7a and d). Even so, in other places it is only half the calculated value (Fig. 7b and d). Two features of the model can be identified as the source of the calculation errors:

- The hybrid differencing scheme used for the convection terms.

Although the hybrid scheme switches to second order accurate central differencing at low velocities, upwind differencing is used for high velocities and large grid sizes. With this type of interpolation the solution is smeared out, rounding off peaks in the solution. Clearly, the model solution exhibits this property of the differencing scheme, e.g. near the top in Fig. 7a, near the bottom of Fig. 7d and at mid height in Fig. 7c.

Borth and Suter [14] also identified this problem of the discretisation scheme in a grid-refinement study of a turbulent flow calculation in a large room. Due to the limitation of computer capacity, grid refinement was not possible in this study.

- The $k-\varepsilon$ turbulence model.

Several author reports that the standard version of the $k-\varepsilon$ model inadequately predicts the turbulence energy k in recirculation zones [8,14,15]. Through its effect on the turbulent viscosity, the local velocity distribution may be different from the actual distribution. This effect may produce the large discrepancy between measurements and model predictions in the centre of the room at mid height (Fig. 7d), which is near the centre of the large recirculation in the empty room.

An important and pronounced difference between measurements and predictions can be found in a horizontal plane at the height of the cooler units. Fig. 8a and b indicate that the trajectory of the jet of air leaving the cooler is not well predicted. At a height of 2.05 m (Fig. 8a) it is seen that the airflow moves towards the side wall after leaving the cooler (the left side on Fig. 8a). The model predicts a straight flow pattern with low velocities near the wall. Furthermore, the magnitude of the air velocity drops as one moves away from the cooler in the z-direction. In reality however the magnitude of the velocity in the jet remains high. This indi-

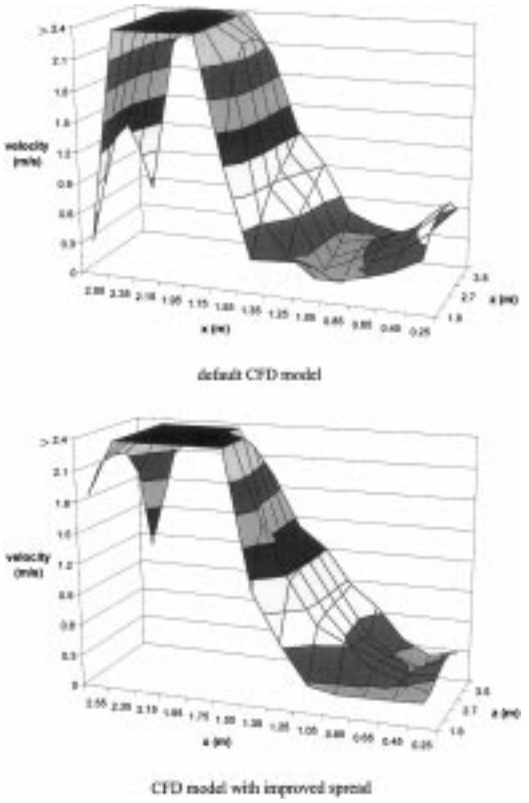

Fig. 10. Comparison between calculated velocity magnitudes with the default CFD model and the improved CFD model with spread in a loaded room at a height of 2.23 m, the x and z dimensions correspond to the dimensions in Fig. 3.

Fig. 10. Comparaison entre les vitesses calculées à l'aide du modèle par défaut CFD et le modèle amélioré avec distribution dans une chambre chargée à une hauteur de 2,23 m ; les dimensions correspondent aux dimensions mentionnées dans la Fig. 3.

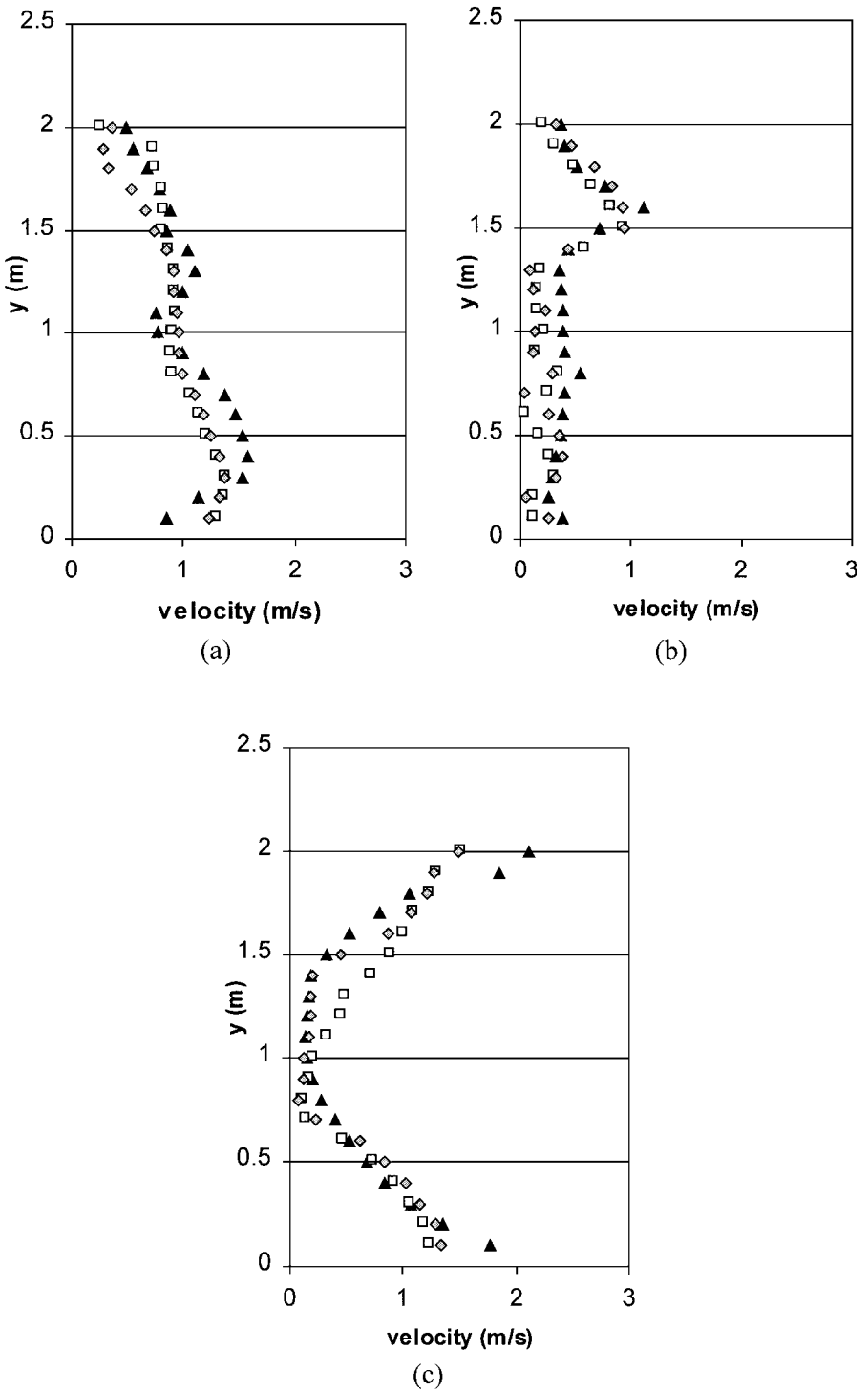

Fig. 11. Comparison between measured (black triangles) and calculated velocity magnitudes with standard $k-\varepsilon$ model (grey diamonds) and RNG $k-\varepsilon$ model (clear squares) at different vertical lines in the room; a, b, c are the positions shown in Fig. 4.

Fig. 11. Comparaison entre les vitesses mesurées (triangles noirs) et calculées avec le modèle standard k−ε (losanges gris) et le modèle k−ε model (clear squares) at different vertical lines in thRNG (carrés blancs) pour différents axes verticaux de la chambre ; a, b et c sont des positions mentionnées dans la Fig. 4.

cates that in the model the airflow drops too soon, while in fact the flow remains attached to the ceiling up to the front wall, where it turns and drops. At a height of 2.23 m (Fig. 8b) the same difference at the side wall is recognised. The jet is also less wide in the predictions, which shows that the spread of the airflow is not predicted accurately. Because in this region a high air velocity is present and a large space is available, turbulence is likely to develop strongly, and may not be predicted well with the standard $k-\varepsilon$ model.

An overall accuracy of 40% is achieved for this case. Mirade reported that the differences between calculated and measured air velocities were 25% of the mean value in an empty meat chiller for a 2D model [6]. For a 3D calculation of a meat chiller filled with objects, the error reported was 40% of the mean value [16]. Harral and Boon [15] found an error of 5% when predicting airflow pattern in a mechanically ventilated livestock building without animals. Here the error was calculated based on the differences between the predicted velocity and measured velocity relative to the bulk jet velocity, which is very high (6.1 m/s) compared to the velocities in the rest of the building.

3.3. Loaded room

The main airflow pattern is similar to that in an empty room (Fig. 6). The air spreads after leaving the cooler unit and flows to the front wall. Due to the occupation of the room by the palloxes, the return path is different. At point c (see Fig. 4), between the palloxes and the wall, there is still a high velocity near the floor and very low velocities at medium height (Fig. 9c), which is comparable to point a in the empty room (Fig. 7a). At point b (Fig. 9b), however, the flow is more uniform as it returns through the channels in between the two rows of palloxes. Looking at a point behind the pallox rows (Fig. 9a), one recognises high velocities at the bottom, at the level of the air gaps between two palloxes and at the top, as a result of the flow through the available channels.

The model prediction for this case is better than for the empty room. An overall accuracy of 30% is obtained. Since the airflow is now constrained to the channels in between palloxes, the turbulence in the flow is not allowed to develop as strongly as in the empty room and therefore plays a less important role for the flow through the channels. However, the space above the palloxes is large enough for turbulence to develop, keeping in mind that the velocity is also high in this region. Indeed, this region has been identified to influence the accuracy of the predictions to a large extend. As was found for the empty room, the air spreads after leaving the cooler unit. When the model is artificially corrected in this region to increase the spread-out of the flow using body force terms at the outlet of the cooler, the prediction is remarkably better (26% accuracy). Fig. 10 shows that the spread of the airflow produces higher velocities near the side wall and a wider jet. In all locations (Fig. 9a–c) the values are closer to the experimental values. This indicates that an accurate prediction of the flow above the palloxes is necessary to improve the predictions around the palloxes. It must be mentioned that the model correction was identified by empirical means. More enhanced models are needed to treat the high velocity turbulent flow.

In an attempt to improve the predictions, the RNG model was applied (Fig. 11) The absolute differences between the measured and calculated velocities were equal to 28.5%, which is higher than that in the standard $k-\varepsilon$ model (26%). The sharp gradient, which the $k-\varepsilon$ model failed to predict, was not improved by the RNG model (Fig. 11b). Near the wall, where the logarithmic wall function was applied, the gradients were not improved either (Fig. 11c). This can be attributed to the wall function and the grid size.

4. Conclusions

This paper presented an industrial application of CFD to an operational cold store for the long-term storage of fruits and vegetables, in which the airflow pattern was investigated. Flexibility has been built in the CFD model with an additional model for the cooler unit. With an average difference of 26% between calculated and measured velocities, it becomes only possible to have a qualitative insight into the airflow pattern for different product stacks, different fan rotation speeds and different room designs, without the need for additional experimental determination of boundary conditions for the velocity. The main deficiencies of the airflow pattern, which cause quality losses in a ventilated space, can be investigated. However, the limited accuracy of the present airflow calculations will not be sufficient to perform detailed calculations of product quality evolution as affected by a cold airflow during long-term storage.

Further fundamental evaluation of the turbulence models and turbulence characteristics of the cold store by means of extensive validation efforts should allow better insight into the model deficiencies. Enhanced turbulence models, such as Reynolds–Stress models are now incorporated in commercial CFD codes and are being more widely validated and could contribute to improved models. The above model incorporating the suggested improvements provides a scientific basis for the simulation of possible solutions to cooling and storage problems. In order to predict the product quality, heat transfer, natural convection and water transport with evaporation and condensation need to be taken into account.

Acknowledgements

The authors wish to thank the Flemish Minister for Science and Technology and the Flanders Institute for the Promotion of the Scientific-Technological Research in the Industry (IWT) for financial support. Author Bart Nicolaï is a research associate with the Flanders Fund for Scientific Research (F.W.O. Vlaanderen).

References

[1] Mirade PS. Contribution á l'amelioration des procédés de traitement des solides par l'air gace à la description et à la simulation de l'aéraulique. Application au réfroidissement et au séchage des viandes, Ph.D. thesis, Université de Poitiers, France, 1996.

[2] Wang H, Touber S. Distributed dynamic modelling of a refrigerated room. Int J Refrig 1990;13:214–22.

[3] Boon CR. Airflow patterns and temperature distribution in an experimental piggery. J Agric Engng Res 1978; 23:129–39.

[4] Van Gerwen RJM, Van Oort H. The use of fluid dynamics simulation models in cold store design. In: Proc. I.I.F.–I.I.R. Commission B2, Bristol, UK, 1989. p. 233–9.

[5] Van Gerwen RJM, Van Oort H. Optimisation of cold store design using fluid dynamics models, Proc. I.I.F.–I.I.R. Commission B2, C2, D1, D2/3, Dresden, Germany, 1989. p. 473–8.

[6] Mirade PS, Daudin JD, Arnaud G. Simulation en deux dimensions de l'aéraulique de deux tunnels de réfrigération des viandes. Int J Refrig 1995;18:403–12.

[7] Mariotti M, Rech G, Romagnoni P. Numerical study of air distribution in a refrigerated room. In: International congress of refrigeration, proceedings, vol. 2, Den Hague, NL, 1995. p. 98–105.

[8] Versteeg HK, Malalasekera W. An introduction to computational fluid dynamics — the finite volume method. New York,: John Wiley and Sons, 1995. p.256

[9] Yakhot V, Orszag SA, Thangam S, Gatski TB, Speziale CG. Development of turbulence models for shear flows by a double expansion technique. Phys Fluids A 1992; 4(7):1510–20.

[10] Zukauskas A, Ulinskas R. Banks of plain and finned tubes. In: Hewitt GF, editor. Handbook of heat exchanger design 2.2.4. London: Hemisphere, 1990. p. 1–17.

[11] Anon. CFX4.1 User manual. Harwell, UK: AEAT, 1995. p. 273-362

[12] Chen Q, Yuan X, Hu Y, Gicksman LR, Yang X. Detailed experimental data of room airflow with displacement ventilation. In: ROMVENT′98: 6th international conference on air distribution in rooms, Pricor, Stockholm, 1998. p. 133–40.

[13] Melikov AK. Accuracy requirements and limitations for low velocity measurements. In: ROMVENT′98: 6th international conference on air distribution in rooms, Pricor, Stockholm, 1998. p. 133–40.

[14] Borth J., Suter P. Influence of mesh refinement on the numerical prediction of turbulent air flow in rooms. In: ROOMVENT′94, vol. 1, Krakow, Poland, 1994. p. 137–48.

[15] Harral BB, Boon CR. Comparison of predicted and measured air flow patterns in a mechanically ventilated livestock building without animal. J Agric Engng Res 1997;66:221–8.

[16] Mirade PS, Daudin JD. Numerical simulation and validation of the air velocity field in a meat chiller. Int J Applied Science and Computations 1998;5(1):11–24.

[17] Launder BE, Spalding DB. The numerical computation of turbulent flow. Computational Methods in Applied Mechanical Engineering ;3:269–89.